An impedimetric study of DNA hybridization on paper-supported inkjet-printed gold electrodes

2014 Nanotechnology 25 094009

(http://iopscience.iop.org/0957-4484/25/9/094009)

IOP Publishing Nanotechnology
Nanotechnology **25** (2014) 094009 (11pp) doi:10.1088/0957-4484/25/9/094009

An impedimetric study of DNA hybridization on paper-supported inkjet-printed gold electrodes

Petri Ihalainen[1], Fredrik Pettersson[2], Markus Pesonen[2], Tapani Viitala[3], Anni Määttänen[1], Ronald Österbacka[2] and Jouko Peltonen[1]

[1] Center of Excellence for Functional Materials and Laboratory of Physical Chemistry, Department of Natural Sciences, Åbo Akademi University, Turku, Finland
[2] Center of Excellence for Functional Materials and Physics, Department of Natural Sciences, Åbo Akademi University, Turku, Finland
[3] Division of Biopharmaceutics and Pharmacokinetics, Faculty of Pharmacy, University of Helsinki, Helsinki, Finland

E-mail: petri.ihalainen@abo.fi

Received 20 June 2013, revised 14 October 2013
Published 12 February 2014

Abstract
In this study, two different supramolecular recognition architectures for impedimetric detection of DNA hybridization have been formed on disposable paper-supported inkjet-printed gold electrodes. The gold electrodes were fabricated using a gold nanoparticle based ink. The first recognition architecture consists of subsequent layers of biotinylated self-assembly monolayer (SAM), streptavidin and biotinylated DNA probe. The other recognition architecture is constructed by immobilization of thiol-functionalized DNA probe (HS-DNA) and subsequent backfill with 11-mercapto-1-undecanol (MUOH) SAM. The binding capacity and selectivity of the recognition architectures were examined by surface plasmon resonance (SPR) measurements. SPR results showed that the HS-DNA/MUOH system had a higher binding capacity for the complementary DNA target. Electrochemical impedance spectroscopy (EIS) measurements showed that the hybridization can be detected with impedimetric spectroscopy in picomol range for both systems. EIS signal indicated a good selectivity for both recognition architectures, whereas SPR showed very high unspecific binding for the HS-DNA/MUOH system. The factors affecting the impedance signal were interpreted in terms of the complexity of the supramolecular architecture. The more complex architecture acts as a less ideal capacitive sensor and the impedance signal is dominated by the resistive elements.

Keywords: electrochemical impedance spectroscopy, printed electronics, paper substrate, DNA, hybridization, surface plasmon resonance

(Some figures may appear in colour only in the online journal)

1. Introduction

Presently, great efforts are being put into the development of paper electronics, both at an academic and an industrial level, with a vision that this could lead to a new generation of low-cost, flexible and robust devices and gadgets. Various electrical components, such as transistors, capacitors, RFID antennas and sensors, have been printed on paper [1–15]. Paper electronics could find applications, for example, in the field of clinical diagnostics, where much focus is currently put on the development of low-cost and robust biosensors applicable as analytical tools for rapid, reliable and sensitive diagnostics of clinically relevant analytes [16]. Screen printing has been a widely applied technique for producing paper-supported devices combined with microfluidic properties [17–19]. Inkjet printing with a higher precision and much lower material

consumption has also proved to be a valuable technique for printed electronics in the field of diagnostics. Recently, the possibility of using paper-supported inkjet-printed gold electrodes in diagnostic applications has been demonstrated, showing that various recognition surfaces can be constructed and clinically relevant analytes can be detected by electrochemical techniques such as electrochemical impedance spectroscopy (EIS) [20–22].

DNA biosensor (genosensor) technologies which can be applied, for example, in the investigation of food and water contamination by micro-organisms, detection of genetic disorders, tissue matching, drug screening and forensic applications, are rapidly developing as an alternative to the classical gene assays [23–27]. In genosensors, the recognition surface combines a single-stranded DNA (ssDNA) probe with a transducer (e.g. optical, mass-sensitive or electrochemical) and utilizes the hybridization event to detect a target DNA sequence [28, 29].

EIS is a very sensitive tool for probing the interfacial properties (capacitance, electron transfer resistance) of surface modified electrodes [30–33]. Since DNA is a polyanionic molecule, hybridization usually results in changes in the electrochemical properties of the interface and thus EIS has been applied for label-free detection of DNA hybridization [28, 29]. For EIS measurements, ssDNA probes have been tethered to metal [34], semiconducting [35–38] and polymeric surfaces [39, 40].

In this study, two different supramolecular recognition architectures for oligonucleotide biosensing are constructed on the paper-supported inkjet-printed gold electrodes. The printed electrodes are fabricated using gold nanoparticle based ink. The first recognition architecture consists of alternate layers of a binary mixture of biotinylated hexa(ethylene glycol) undecane thiol (Biotin-PEG-thiol) and 11-mercapto-1-undecanol (MUOH) (85:15 mol%,) self-assembled monolayer (SAM), streptavidin (SA) and biotinylated DNA probe (biotin-DNA probe). The other recognition architecture is constructed by subsequent immobilization of a thiol-functionalized DNA probe (HS-DNA probe) and 11-mercapto-1-undecanol (MUOH). The binding capacity and selectivity of the recognition architectures were studied by surface plasmon resonance (SPR). The feasibility of these architectures on paper-supported electrodes for the detection of DNA hybridization by EIS is screened.

2. Materials and methods

2.1. Print substrate

A proprietary multi-layer laboratory-coated paper developed for printed electronics was used as print substrate [41]. The paper contains the following layers: ground calcium carbonate (GCC) precoated on wood-free base paper, a laboratory-blade-coated kaolin layer, a reverse gravure-coated barrier layer and a thin nanoporous precipitated calcium carbonate (PCC) pigment top coating layer (layer thickness ~3 μm). The paper contains components normally used in papermaking and is similarly recyclable to the ordinary paper used in graphical printing. The most important physicochemical characteristics and examples of numerous applications in the field of printed electronics are described in previous publications [1, 2, 4–9, 11, 20–22, 42]. The total thickness and grammage of the paper substrate were about 130 μm and 126 g m^{-2}, respectively. A more detailed description of the layer components and preparation procedures of the paper substrate used here are given elsewhere [8].

2.2. Inkjet printing of AuNP electrodes

Dodecanethiol-stabilized gold nanoparticles (AuNPs) with an average size distribution of ~7 nm were synthesized following the procedure reported by Hostetler *et al* [43]. Detailed information about the synthetic steps of these AuNPs is given elsewhere [20]. All chemicals used in synthesis were purchased from Sigma-Aldrich and used without further purification. The AuNP ink for inkjet printing was prepared by dispersing the nanoparticles (15 wt%) in xylene (Sigma-Aldrich). Inkjet printing of the AuNP ink was performed with a Dimatix Materials Printer (DMP-2800, FUJIFILM Dimatix, Inc. Santa Clara, USA). The printing was done in ambient conditions using a single nozzle, 10 pl drop volume, 27 ± 3 V firing voltage and a custom waveform to ensure optimal droplet formation. Printing was performed using a drop spacing of 20 μm. Sintering of the printed gold electrodes was carried out using a short-wave IR drier (IRT systems, Hedson Technologies AB, Sweden) consisting of three 30 cm-long 2 kW strip light bulbs with the distance between the sample and the lamp being about 20 cm. The sintering time was 20 s. The volume resistivity of the printed gold structures was 1.6×10^{-7} Ω m. The thickness of the gold layer was about 500 nm. Two different electrode configurations were prepared, with an active area of 0.28 cm^2 [20] or 0.08 cm^2. A photograph of a paper-supported printed electrode with an active area of 0.08 cm^2 is shown in figure 1. The average RMS roughness of the electrode surface was 27 nm (measured from 5 μm × 5 μm atomic force microscope (AFM) topographs). A more detailed description of the fabrication, characterization and surface modification of the paper-supported inkjet-printed gold electrodes is given in previous communications [4, 20–22].

A hydrophobic and translucent polydimethylsiloxane (PDMS) based ink (Dehesive 920, catalyst OL and crosslinker V24, mixing ratio of 100:2.5:1 wt%, Wacker Chemie, AG) was applied around the perimeter of the electrodes to confine the aqueous sample solutions over the electrode area during the preparation of recognition layers and impedance measurements [20]. The PDMS ink can be applied on a paper substrate by manual spreading or by using roll-to-roll compatible techniques such as flexographic or inkjet printing [44].

2.3. Alkylthiols, proteins and oligonucleotides

11-Mercapto-1-undecanol (MUOH, $HS(CH_2)_{11}OH$) was purchased from Sigma-Aldrich. Biotinylated hexa(ethylene glycol) undecane thiol (Biotin-PEG-thiol, $HS(CH_2)_{11}(OCH_2CH_2)_6NHBiotin$) was obtained from nanoScience Instruments (Phoenix, USA). The thiols were used as received. Streptavidin (SA) was purchased from BioSPA (SPA Società

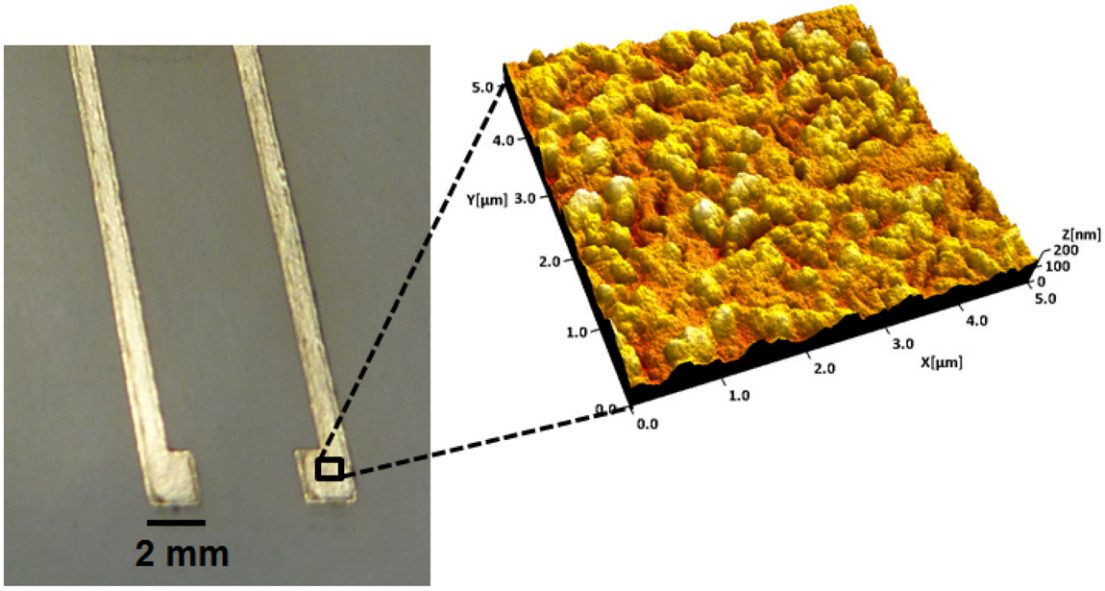

Figure 1. A paper-supported printed gold electrode with an active area of 0.08 cm^2 (small squares). Also shown is a small-scale AFM image (5 μm × 5 μm) of the electrode surface.

Prodotti Antibiotici S.p.A., Italy). The following oligonucleotides were obtained from biomers.net:
Biotinylated DNA probe (biotin-DNA probe, sequence 5′ → 3′ aaACTGAATTATTGGAGGTAGAGGTGAGTGATAC, biotin linker at 5′ end, MW 11 072 g mol^{-1}).

Complementary DNA target (sequence 5′ → 3′ aaGTATCACTCACCTCTACCTCCAATAATTCAGT, biotin linker at 5′ end, MW 10 703 g mol^{-1}).

Non-complementary DNA target (sequence 5′ → 3′ aaTAGCTAGTCAGTATATAGCTTAGCTAGCTAGA, MW 10 927 g mol^{-1}).

Thiol-functionalized DNA probe (HS-DNA probe, sequence 5′ → 3′ aaACTGAATTATTGGAGGTAGAGGTGAGTGATAC, alkylthiol linker at 5′ end, MW 10 832 g mol^{-1}).

4-(2-hydroxyethyl)-1-piperazineethanesulfonic acid (HEPES)–ethylenediaminetetraacetic acid (EDTA) aqueous solution (10 mM HEPES (Sigma), 300 mM NaCl (Fluka), 1 mM EDTA (Sigma), pH 7.4) was used as a buffer solution in all the immobilization experiments and impedance measurements.

2.4. Formation of supramolecular protein architectures on printed AuNP electrodes

Two well-known supramolecular architectures were used for fabrication of the recognition layers for DNA hybridization experiments (figure 2). In the first one, the biotin-DNA probe molecules are tethered to an SA layer coupled to the biotinylated SAM [45–47]. The other one is based on the mixed SAM of HS-DNA probe and MUOH [45, 48, 49].

2.4.1. Formation of MUOH:Biotin-PEG-thiol SAM-SA-biotin-DNA probe architecture. The first layer consisted of a biotinylated SAM formed using MUOH:Biotin-PEG-thiol (85:15 mol%, 5 mM) solution in absolute ethanol (ETAX Aa, Altia). Before exposure to a SAM solution, the AuNP electrodes were cleaned with plasma (air) flow (PDC-326, Harrick) for 2 min, rinsed with absolute ethanol and dried with nitrogen gas. The paper-supported electrodes were sealed between two silicon rings in a custom built liquid flow cell (FIAlab Instruments, Inc., USA) with a cap and exposed to SAM solution (250 μl) for 19–23 h at room temperature in the dark. After SAM formation, the electrodes were removed from the solution, rinsed immediately with absolute ethanol, and dried with nitrogen gas. Samples were stored at +6 °C until further analysis.

The second layer was formed by pipetting 50 μl of SA solution (HEPES–EDTA buffer, 5 μg ml^{-1}) over the MUOH:Biotin-PEG-thiol covered electrode area. The immobilization was conducted at +4 °C for 12 h. After immobilization, the electrode surface was rinsed with the HEPES–EDTA buffer solution and pure water (MilliQ) and dried with nitrogen gas. Samples were stored at +6 °C until further analysis.

The biotin-DNA probe molecules were immobilized by applying 50 μl of DNA solution (HEPES–EDTA buffer, 100 nM) over the electrode area. The immobilization was conducted at +4 °C for 12 h. After immobilization, the electrode surface was rinsed with the HEPES–EDTA buffer solution and pure water (MilliQ) and dried with nitrogen gas. Samples were stored at +6 °C until further analysis.

The complementary and non-complementary target DNA analyte molecules were immobilized on the recognition layer by applying 50 μl of DNA solution (HEPES–EDTA buffer, 100 nM, 4 pmol) over the electrode area. The hybridization was conducted at RT for 3 h. After immobilization, the electrode surface was rinsed with buffer solution and pure water (MilliQ) and dried with nitrogen gas. Samples were stored at +6 °C until further analysis.

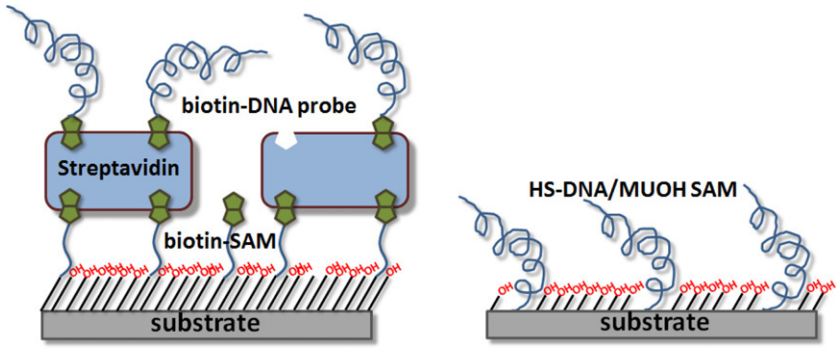

Figure 2. Schematic illustrations of the supramolecular architectures used as the recognition layers. Left: MUOH:Biotin-PEG-thiol SAM-SA-biotin-DNA probe recognition architecture. Right: mixed HS-DNA probe and MUOH SAM architecture.

2.4.2. Formation of the mixed HS-DNA probe and MUOH SAM architecture. Mixed HS-DNA probe and MUOH SAM layers were assembled by a two-step backfilling process [45, 48, 49]. First, pure DNA probe monolayers were prepared by placing a 50 μl drop of SH-DNA solution over an electrode area for 5 h. After HS-DNA assembly, the samples were rinsed thoroughly with buffer and pure water (MilliQ) to remove loosely bound HS-DNA. Then, a 50 μl drop of diluent MUOH solution (10 μM in water) was applied for 1 h. After the MUOH backfilling, the samples were removed from the solution, rinsed thoroughly with pure water (MilliQ), and dried under nitrogen gas flow. Samples were stored at +6 °C until further analysis.

The complementary and non-complementary target DNA analyte molecules were immobilized on the recognition layer by applying 50 μl of DNA solution (HEPES–EDTA buffer, 100 nM, 4 pmol) over the electrode area. The hybridization was conducted at RT for 3 h. After immobilization, the electrode surface was rinsed with buffer solution and pure water (MilliQ) and dried with nitrogen gas. The samples were stored at +6 °C until further analysis.

2.5. Contact angle measurements

A CAM 200 contact angle goniometer (KSV Instruments Ltd, Finland) was used for the determination of contact angles. The contact angles of water (Millipore) on the sample surfaces were measured in air in ambient conditions (RH = 23 ± 5%, $T = 25 \pm 3$ °C). Measured contact angle values were obtained at the point where the contact diameter of the drop, contact angle and volume remained constant. The contact angles were calculated using the software supplied with the instrument, which utilizes both a circular and a Laplace fit to the projected drop curvature. The volume of the droplets was 2 μl.

2.6. Atomic force microscopy

An NTEGRA Prima (NT-MDT, Russia) atomic force microscope (AFM) was used to analyze the topography of the samples in intermittent-contact mode. The images (1024 pixels × 1024 pixels) were captured in ambient conditions (RH = 20–26%, $T = 24$–28 °C) using silicon cantilevers with a nominal tip radius of 10 nm (Model: NSG10, NT-MDT, Russia). The scanning rate and damping ratio were 0.39 Hz and 0.6–0.7, respectively. Image analysis was done using SPIP^{TM} image analysis software (Image Metrology, Denmark).

2.7. Surface plasmon resonance

Surface plasmon resonance (SPR) gold slides were coated with recognition layers exactly with the same procedure as described for the printed gold electrodes. DNA hybridization was monitored *in situ* with a multi-parametric SPR instrument (SPR Navi 200, Bionavis Ltd, Tampere, Finland). The SPR Navi 200 instrument has an integrated peristaltic pump and a sample loop system connected to a six-port valve, which allows injection of sample plugs into the continuously running buffer. For measurements, the flow channel of the SPR system was first filled with HEPES–EDTA buffer with a constant flow rate of 20 μl min^{-1}. After a stable baseline was achieved, DNA target solutions were injected as a plug into the continuously flowing buffer stream to measure the interaction.

2.8. Impedance measurements

Impedance measurements were done on the paper-supported gold electrodes functionalized with a MBP SAM and protein layers in contact with the electrolyte HEPES–EDTA buffer solution. Buffer solution (50 μl) was deposited on the electrode area exactly at the same spot which had been functionalized with the recognition layers. Electrical impedance spectroscopy is a powerful tool to investigate the movement and reactions of charged species in an electrochemical cell [50]. The general idea is to apply a time varying electrical signal to the electrodes and measure the response. The two parameters that are measured are the phase shift (θ) between the input and output signals and the change in signal amplitude or modulus, $|Z| = R_M V_{IN}/V_{OUT}$, where R_M is the measuring resistance. These changes depend on all charged species in the system, i.e. ion movement in the dielectric, electron movement in the electrodes, redox processes, etc, as well as on the surface roughness of the electrode. The total impedance consists of a resistive, a capacitive and an inductive component and is therefore dependent on the frequency of the probe signal. Different processes (dipolar, electronic, and ionic saturation)

have different time responses and the impedance is therefore measured over a wide range of frequencies, usually ranging from 1 MHz to 1 mHz. All the measurements in this paper are potentiostatic, i.e. an actuating voltage is applied and the current is measured. No equivalent circuit has been used to model the system after the measurements. The presented values are the impedance of the entire measuring cell. The reason for not including an equivalent cell and calculating, for instance, the capacitance of each individual interface in the device is the simplicity. The signals being monitored must be strong enough so that complex analysis of the acquired data is minimized. In order to calculate the capacitance and real and imaginary impedance, θ and $|Z|$ is separated into its real and imaginary parts. $Z = Z_{\text{real}} + Z_{\text{img}} = |Z|e^{-i\theta}, \theta = \tan^{-1}(Z_{\text{img}}/Z_{\text{real}})$ and $|Z| = ((Z_{\text{real}})^2 + (Z_{\text{img}})^2)^{1/2}$, where Z_{real} is the real and Z_{img} is the imaginary impedance. The capacitance then comes to $C = -1/(-Z_{\text{img}} 2\pi f A)$, where f is the frequency and A is the capacitor area. The instrument used was a Gamry 600 Impedance Spectrometer. In all measurements the connection used was tripolar, the frequency was scanned from 1 Hz to 1 MHz and the alternating voltage applied to the electrodes had an rms amplitude of 20 mV and 0 V contact bias voltage. Between the application of buffer solution on the dry electrode area and the start of the impedance measurements, it was necessary to wait 10–15 min before reaching a stable baseline signal.

3. Results and discussion

3.1. Binding capacity and selectivity of recognition architectures

The binding capacities and selectivity of the MUOH:Biotin-PEG-thiol SAM-SA-biotin-DNA probe and mixed HS-DNA probe and MUOH SAM recognition architecture were determined separately by SPR. Figure 3 shows the difference in SPR signal between complementary and non-complementary DNA targets for both recognition architectures after injection of a 100 nM concentration of target sample. A higher relative SPR signal indicates better selectivity of the MUOH:biotin-PEG-thiol SAM-SA-biotin-DNA probe system compared to the recognition architecture with a mixed HS-DNA probe and MUOH SAM. In absolute terms, the binding capacity of the MUOH:biotin-PEG-thiol SAM-SA-biotin-DNA probe system towards the complementary DNA target was 5:7–7:4 ng cm^{-2} and towards the non-complementary DNA target was 1:1 ng cm^{-2}. Thus, the signal specificity is over 80%. For the other system, the binding capacity towards the complementary DNA target was 7.4–8.1 ng cm^{-2} but with a very high unspecific background (∼65%) towards the non-complementary DNA target. SA based recognition platforms have been shown to be more sensitive, with much lower background signals from unspecific binding compared to DNA SAM based systems [45]. SA is known to have excellent anti-fouling characteristics towards biomolecules due to its highly hydrophilic surface properties, preventing the approach of biomolecules closer than 3 nm from the SA layer [51].

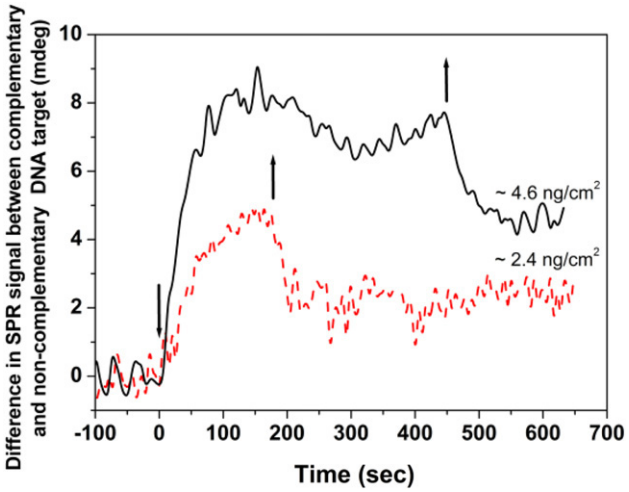

Figure 3. Difference in surface plasmon resonance (SPR) signal between complementary and non-complementary DNA targets for MUOH:Biotin-PEG-thiol SAM-SA-biotin-DNA probe (solid line) and mixed HS-DNA probe and MUOH SAM (dashed line) recognition architectures. The down arrow represents the time of DNA target injection (100 nM) and the up arrow indicates the injection of HEPES–EDTA buffer without DNA.

3.2. Impedimetric analysis of DNA hybridization in MUOH:Biotin-PEG-thiol SAM-SA-biotin-DNA probe architecture

Figure 4 shows the Bode plots of (a) impedance modulus $|Z|$ and (b) phase angle as a function of frequency after immobilization of each successive layer on the printed AuNP electrode. Also included are the (c) real (Z_{real}) and (d) imaginary (Z_{img}) components of impedance. These describe the resistive (real part) or capacitive (imaginary part) properties of the system. The area of the electrode used for these experiments was 0.28 cm^2. The Z_{real} value being higher than the Z_{img} value in the higher frequency domain (>10 kHz) shows that the resistive properties primarily control the impedance over the capacitive properties at these frequencies.

Figure 4(a) shows that each additional molecular layer decreases the impedance modulus in the higher frequency region (>10 kHz). The same trend is observed in the Z_{real}-curve. At the lower frequency domain, the $|Z|$ value first increases after the addition of MUOH:Biotin-PEG-thiol SAM and then slightly decreases with each additional biomolecular layer. Again, the same trend is observed for Z_{real}. In the Z_{img} curve, the addition of MUOH:Biotin-PEG-thiol SAM shifts the impedance upwards throughout the whole measured frequency range. This indicates a decrease in capacitance of the system. After immobilization of the subsequent biomolecular layers, the Z_{img} values flocculate over and below that of MUOH:Biotin-PEG-thiol SAM and do not show a clear trend. The phase angle plot shifts downwards after the addition of MUOH:Biotin-PEG-thiol SAM, especially at lower frequencies, and for additional biomolecular layers does not change considerably. Comparison between the hybridization with complementary (figure 4(a)) and non-complementary DNA targets (figure 5(a)) shows that changes in the $|Z|$ signals

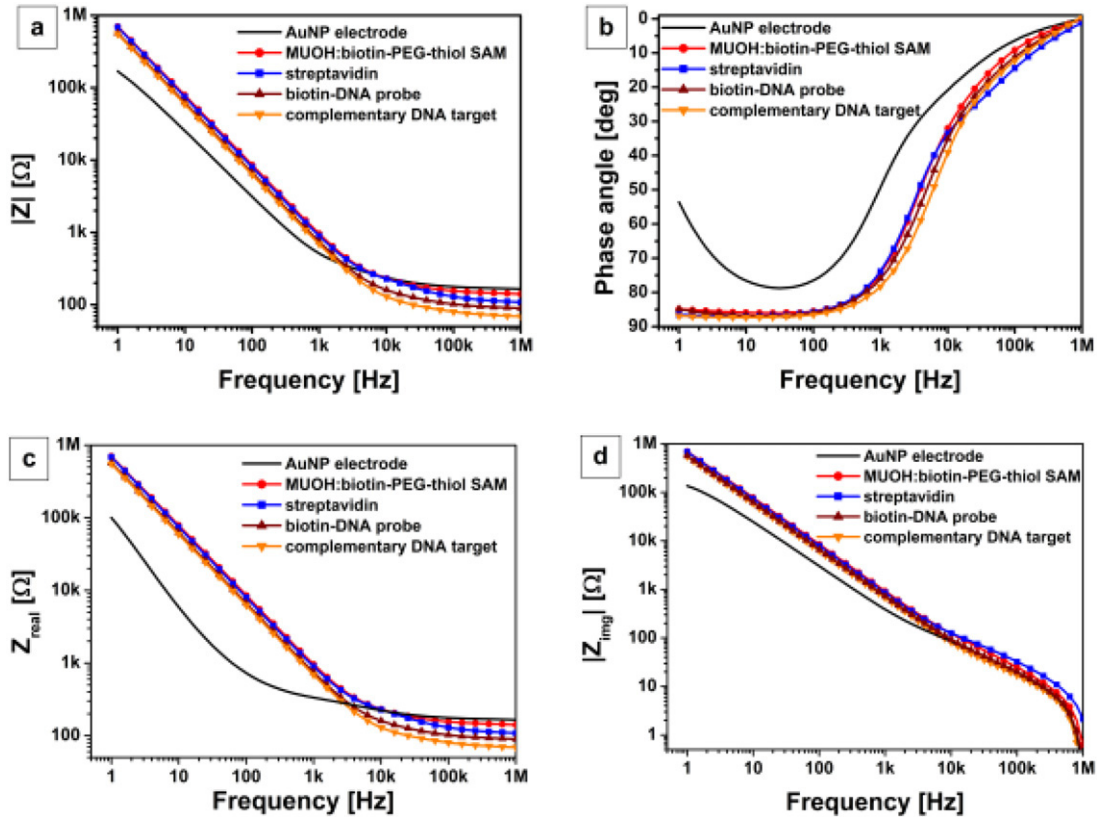

Figure 4. (a) Bode plot of impedance modulus $|Z|$ and (b) phase angle as a function of frequency after each immobilization step for the MUOH:Biotin-PEG-thiol SAM-SA-biotin-DNA probe recognition architecture and after hybridization with the complementary DNA target. Also shown are the corresponding curves for the (c) real (Z_{real}) and (d) imaginary (Z_{img}) components of impedance as a function of frequency. The electrode area was 0.28 cm^2.

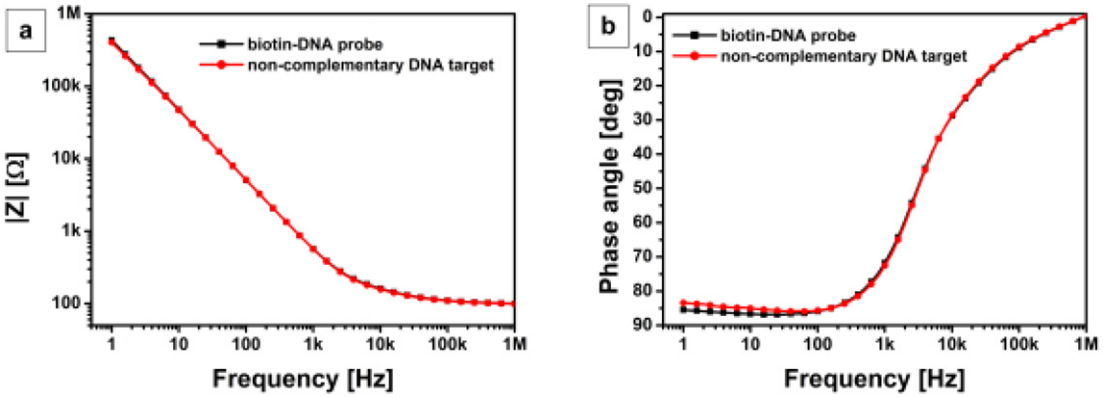

Figure 5. (a) Bode plot of the impedance modulus $|Z|$ and (b) phase angle as a function of frequency for the MUOH:Biotin-PEG-thiol SAM-SA-biotin-DNA probe recognition architecture before and after hybridization with the non-complementary DNA target. The electrode area was 0.28 cm^2.

in the higher frequency region are apparent for the former and negligible for the latter. Only a small shift in phase angle is observed at low frequencies (figure 5(b)). This indicates good selectivity of the EIS signal in the MUOH:Biotin-PEG-thiol SAM-SA-biotin-DNA probe recognition architecture. The above is in agreement with the SPR results.

The interface between the metal electrode and electrolyte with an adsorbed biomolecular layer can be usually described by three physical regions: bulk solution, double layer and molecular layer [30, 31, 37, 38]. The contribution to the total impedance signal can be considered to arise from the uncompensated solution resistance, and the resistance and capacitance of the biomolecular layer and electric double layer at the electrode/electrolyte interface. An electric double layer is generated when charge species and dipoles are orientated at the surface of the metal electrode in contact with an electrolyte. A compact Helmholtz plane or a Stern layer is formed by the solvent and adsorbed species in the vicinity of

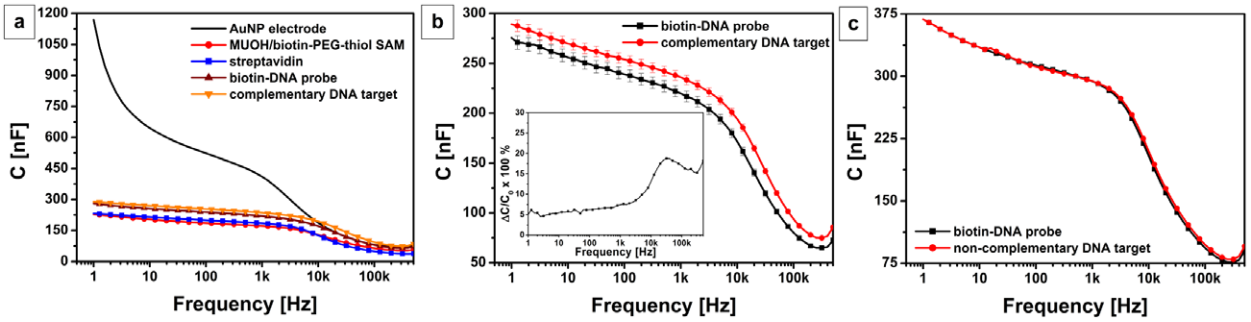

Figure 6. (a) Capacitance (C) as a function of frequency after each immobilization step for the MUOH:Biotin-PEG-thiol SAM-SA-biotin-DNA probe recognition architecture and after hybridization with the complementary DNA target. (b) C as a function of frequency for SAM-SA-biotin-DNA probe recognition architecture before and after hybridization with the complementary DNA target (with error bars). The inset shows the relative change in capacitance ($\Delta C/C_0$) as a function of frequency. (c) C as a function of frequency for the SAM-SA-biotin-DNA probe recognition architecture before and after hybridization with the non-complementary DNA target. The electrode area was 0.28 cm^2.

the electrode surface, and the thickness of the double layer determines how close the solvated ions from the bulk solution can approach. Due to the surface heterogeneities, the double layer is not a well defined discrete element, but consists of parallel or branched resistive–capacitive transmission lines. The adsorbing molecules will displace water and solvated ions, moving the electric double layer outwards from the electrode surface, resulting in a change of the capacitance. The capacitance of the adsorbed layer depends on the dielectric constant and thickness. The resistive component is introduced by the defects, enabling the penetration of electrolyte and migration of ions through the molecular layer. Among the factors influencing the uncompensated resistance are the shape and size of the cell, the location of the reference electrode, the shape of the working electrode, and the size and position of the counter-electrode [52].

Alkyl thiol SAMs have been shown to be good electronic insulators and decrease the capacitance of metal electrodes [53, 54]. The insulation characteristics of the MUOH:Biotin-PEG-thiol SAM is indicated by the increase in Z_{real} in the lower frequency domain (<10 kHz). The decreasing effect on capacitance is shown by the C versus frequency curve (figure 6(a)), a drop again seen at lower frequencies. Although SAMs are generally good electronic insulators, they are not necessarily good ionic insulators [54]. The ionic insulator characteristics of SAMs can be assessed by studying the phase angle plot in the lower frequency region [54]. Theoretically, SAMs obey the Helmholtz ideal capacitor model when the phase angle at 1 Hz is 90° [50]. On the other hand, phase values ≥88° can be used as a reliable indicator of the perfect ionic insulating character of a SAM [54]. After the immobilization of MUOH:Biotin-PEG-thiol SAM, the phase angle value is around 85° at 1 Hz (figure 4(b)). This indicates that MUOH:Biotin-PEG-thiol SAM is not completely defect-free and acts as a capacitor contaminated by a resistive component associated with current leakage at defect sites. The decrease in resistance compared to the pristine AuNP electrode in the higher frequency domain might be due to the increased wettability of the surface. Higher wettability leads to better penetration of the electrolyte and the enhanced migration of ionic species. The pristine AuNP electrode is a quite poor wetting surface, the contact angle of water being about 86°–90° [4]. This has been attributed to the residual hydrophobic dodecanethiol surfactant molecules still adsorbed on the surface. When MUOH:Biotin-PEG-thiol SAM is adsorbed on the surface, the wetting properties of the electrodes are considerably enhanced and the contact angle decreases to 40°.

After the addition of subsequent biomolecular layers, $|Z|$ and Z_{real} decrease throughout the whole measured frequency range (figure 4). The effect is more pronounced at higher frequencies. In addition, the C curve shows an increase (figure 6(a)). The decrease in impedance has been observed both in antibody–antigen interactions and DNA hybridization reactions [37–40, 55]. All the biomolecules have surface charges and the immobilization of the biomolecules to the metal electrode surface changes the charge distribution in the electrical double layer at the solid/liquid interface. Changes in the charge distribution affect the migration of ionic species through the double layer. This in turn changes the resistance of the biomolecular layer. In particular, DNA hybridization has been shown to increase the surface conductivity [56]. The decreasing effect of biomolecule adsorption on impedance is shown to be more pronounced at higher frequencies for systems using alkyl chain SAMs as tethering surfaces for biomolecules [37, 38]. This is attributed to the overall high resistance of SAM, which dominates the signal at lower frequencies and makes the change in total resistance hard to detect [40].

The hybridization with the complementary DNA target induces a clear increase in capacitance throughout the whole measured frequency range (figure 6(b)). The largest relative change in C is observed at around 3.5 kHz, with an approximately 20% increase in signal (the inset of figure 6(b)). On the other hand no change was observed with the non-complementary DNA target (figure 6(c)). The adsorption of biomolecules has been shown to influence the capacitance of the double layer to varying degrees [30, 31]. Both decreases and increases in capacitance have been observed, the phenomenon attributed to the change in thickness, charge

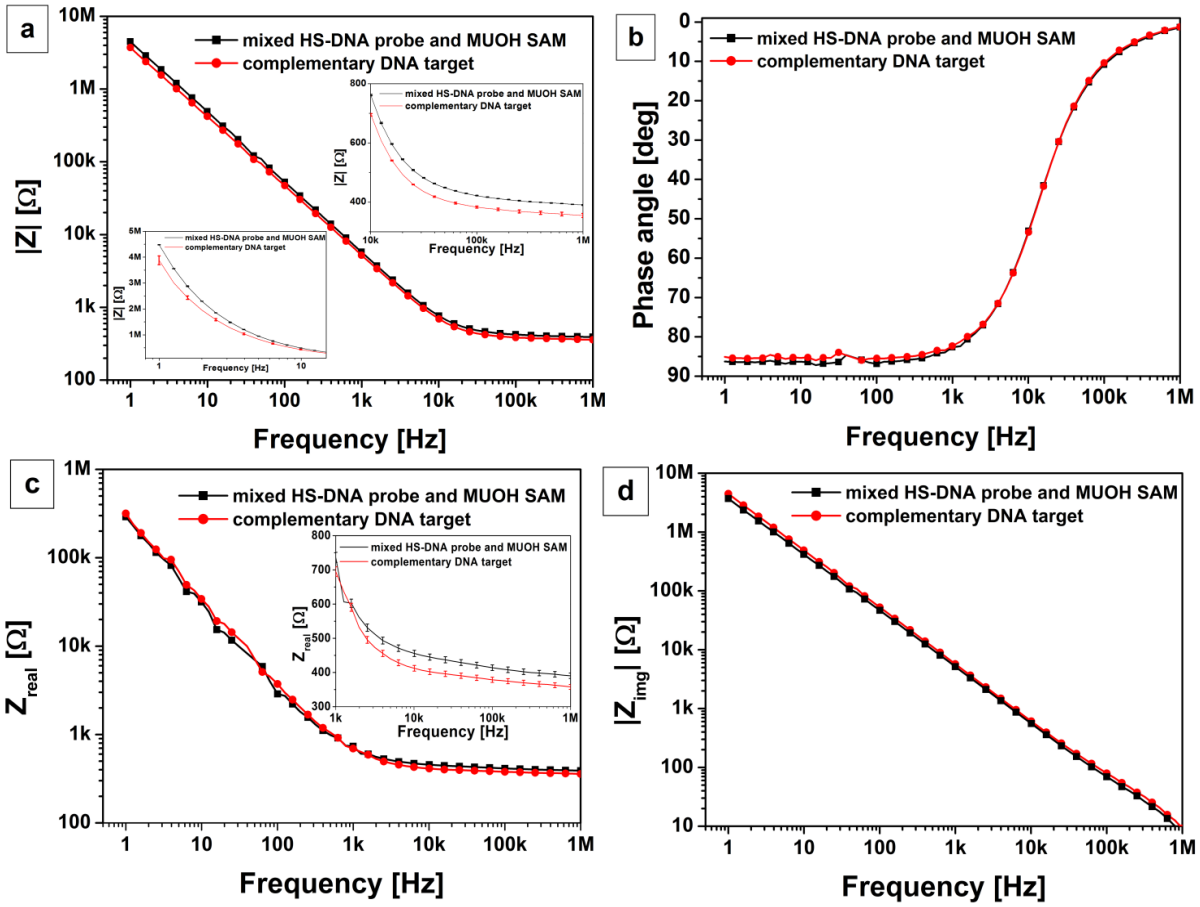

Figure 7. (a) Bode plot of the impedance modulus $|Z|$ and (b) phase angle as a function of frequency for the mixed HS-DNA probe and MUOH SAM recognition architecture before and after hybridization with the complementary DNA target. Also shown are corresponding curves for the (c) real (Z_{real}) and (d) imaginary (Z_{img}) components of impedance as a function of frequency. The insets of (a) and (c) show linear–log plots (including error bars) of the corresponding curves with a zoomed-in scale. The electrode area was 0.08 cm^2.

exchange, change in conformation, and interpenetration of biomolecules into the dielectric layer [20, 34–36, 40, 55, 57–61]. The increase in capacitance after adsorption of biomolecules is especially seen for systems with porous and less ideal dielectric layers [20, 40, 55, 57, 61]. This has been attributed to the interpenetration of biomolecules to the dielectric layer and the change in the effective dielectric constant of the layer.

3.3. Impedimetric analysis of DNA hybridization in the mixed HS-DNA probe and MUOH SAM architecture

Figure 7 shows the Bode plots of (a) $|Z|$ and (b) phase angle as a function of frequency before and after DNA hybridization with the complementary DNA target. Also included are the (c) Z_{real} and (d) Z_{img} components of impedance. Figure 8 shows (a) $|Z|$ and (b) phase angle curves for the non-complementary DNA target. Figure 9 shows C as a function of frequency both for (a) complementary and (b) non-complementary DNA targets.

The $|Z|$ curve shows a very small decrease after DNA hybridization with the complementary DNA target (figure 7(a) and the inset of figure 7(a)). No noticeable change is observed for the non-complementary DNA target (figure 8(a)). Figure 7(c) (and corresponding inset) shows that the decrease in impedance is also seen in the Z_{real} curve, but only in the higher frequency domain (>10 kHz). On the other hand, the Z_{img} curve does not show any significant change after DNA hybridization (figure 7(d)). However, the most noticeable change is observed in the C curve with the complementary DNA target (figure 9(a)). The largest increase in signal (∼13%) is observed at around 1 Hz and 200 kHz (the inset of figure 9(a)). Again, no change is observed for the non-complementary DNA target (figure 9(b)). This indicates a good selectivity of the EIS signal in the mixed HS-DNA probe and MUOH SAM system. However, this is in disagreement with SPR results, which showed a very high background signal from the non-complementary DNA target. However, the direct comparison between SPR and EIS is difficult due to the different physical principles of the two techniques.

The changes in the impedance signals after DNA hybridization for the mixed HS-DNA probe and MUOH SAM system are similar to the MUOH:Biotin-PEG-thiol SAM-SA-biotin-DNA probe architecture, i.e. a decrease in resistance and an increase in capacitance. In addition, the selectivity of the EIS signal is also comparable between the two recognition systems. The mixed HS-DNA probe and MUOH SAM system

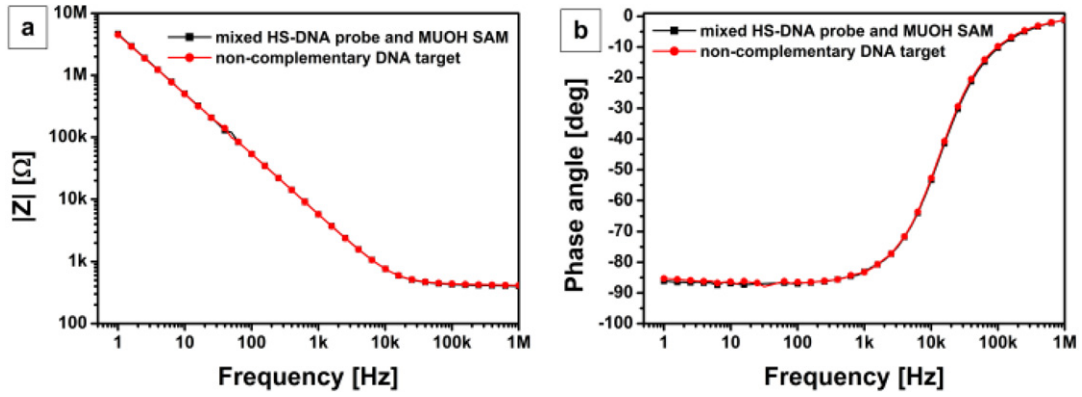

Figure 8. (a) Bode plot of the impedance modulus $|Z|$ and (b) phase angle as a function of frequency for the mixed HS-DNA probe and MUOH SAM recognition architecture before and after hybridization with the non-complementary DNA target. The electrode area was 0.08 cm^2.

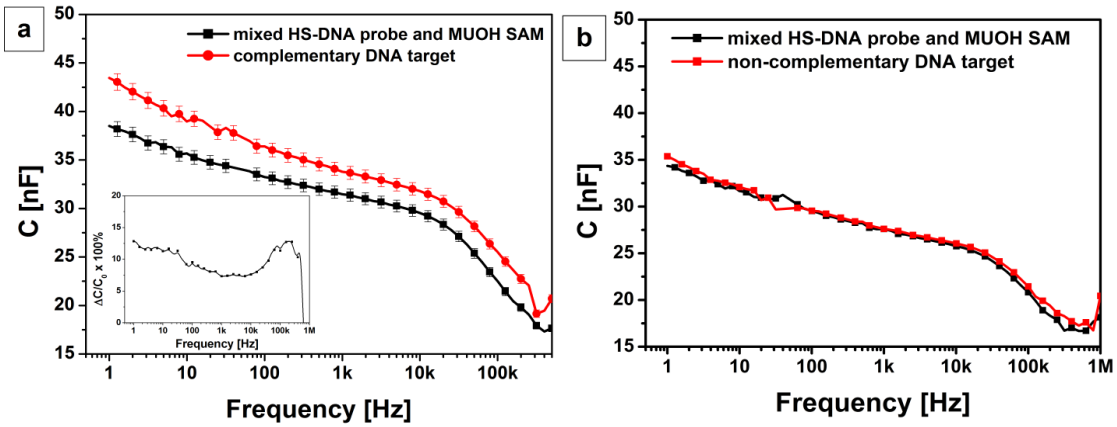

Figure 9. (a) C as a function of frequency for the mixed HS-DNA probe and MUOH SAM recognition architecture before and after hybridization with the complementary DNA target. The inset shows the relative change in capacitance ($\Delta C/C_0$) as a function of frequency. (b) C as a function of frequency for the HS-DNA probe and MUOH SAM recognition architecture before and after hybridization with the non-complementary DNA target. The electrode area was 0.08 cm^2.

shows a relatively higher increase in the C signal after the hybridization with the complementary DNA target compared to the MUOH:Biotin-PEG-thiol SAM-SA-biotin-DNA probe architecture. The higher EIS signal for the former is consistent with the higher binding capacity observed with SPR. However, the MUOH:Biotin-PEG-thiol SAM-SA-biotin-DNA probe system has the highest relative change in C around 3.5 kHz, the change being 20%.

4. Conclusions

The current study demonstrates that different supramolecular architectures for DNA hybridization can be successfully formed on paper-supported AuNP electrodes. The DNA hybridization can be detected with impedimetric spectroscopy in the picomol range. The EIS results indicated a good selectivity for both recognition architectures, whereas SPR showed very high unspecific binding for the mixed HS-DNA probe and MUOH SAM system. In addition, SPR results showed that the mixed HS-DNA probe and MUOH SAM system had a higher binding capacity towards the complementary DNA target. This coincides with the magnitude of change in the EIS signal in the lower frequency region, which is dominated by changes in capacitance. However, the MUOH:Biotin-PEG-thiol SAM-SA-biotin-DNA probe system has the highest change in C around 3.5 kHz, with the relative change being 20%. The factors affecting the impedance signal and complexity of the interpretation is at least partly linked to the complexity of the supramolecular architecture. Although the changes in impedance signals after DNA hybridization are more apparent in the more complex system (i.e. MUOH:Biotin-PEG-thiol SAM-SA-biotin-DNA probe), it is also less ideal for fabrication of a capacitive genosensor due to the more dominant resistive elements. In addition, producing the recognition surfaces, for example, by printing would benefit from simpler recognition architectures. Further work is in progress towards the development of a low-cost and recyclable paper electronics platform for genosensor applications.

Acknowledgments

The SalWe IMO programme (Project number: 648/10) funded by the Finnish Funding Agency for Technology and Innovation

(TEKES) is acknowledged for financial support. Tapani Viitala wishes to acknowledge support from the Academy of Finland (grants 137053 and 263861). Björn Törngren (Åbo Akademi) is thanked for synthesis of AuNP nanoparticles. Markku Syrjänpää (Turku University) is acknowledged for providing the oligonucleotides.

References

[1] Hassinen J, Kauppila J, Leiro J, Määttänen A, Ihalainen P, Peltonen J and Lukkari J 2013 Low-cost reduced graphene oxide based conductometric nitrogen dioxide sensitive sensor on paper *Anal. Bioanal. Chem.* **405** 3611–7

[2] Sarfraz J, Ihalainen P, Määttänen A, Lindén M and Peltonen J 2013 Printed hydrogen sulfide gas sensor on paper substrate based on polyaniline composite *Thin Solid Films* **534** 621–8

[3] Ihalainen P, Määttänen A, Järnström J, Tobjörk D, Österbacka R and Peltonen J 2012 Influence of surface properties of coated papers on printed electronics *Indust. Eng. Chem. Res.* **51** 6025–36

[4] Määttänen A, Ihalainen P, Pulkkinen P, Wang S, Tenhu H and Peltonen J 2012 Inkjet-printed gold electrodes on paper—characterisation and functionalisation *ACS Appl. Mater. Interfaces* **4** 955–64

[5] Sarfraz J, Määttänen A, Ihalainen P, Keppeler M, Lindén M and Peltonen J 2012 Printed copper acetate based H_2S sensor on paper substrate *Sensors Actuators* B **173** 868–73

[6] Tobjörk D *et al* 2012 IR-sintering of ink-jet printed metal-nanoparticles on paper *Thin Solid Films* **520** 2949–55

[7] Tobjörk D and Österbacka R 2011 Paper electronics *Adv. Mater.* **23** 1935–61

[8] Ihalainen P, Määttänen A, Mattinen U, Stępień M, Bollström R, Toivakka M, Bobacka J and Peltonen J 2011 Electrodeposition of PEDOT-Cl film on a fully printed Ag/polyaniline electrode *Thin Solid Films* **519** 2172–5

[9] Saarinen J J, Ihalainen P, Määttänen A, Bollström R and Peltonen J 2011 Printed sensor and electric field assisted wetting on a natural fibre based substrate *Nord. Pulp Pap. Res. J.* **26** 133–41

[10] Unander T and Nilsson H-E 2009 Characterization of printed moisture sensors in packaging surveillance applications *IEEE Sensors J.* **9** 922–8

[11] Bollström R, Määttänen A, Tobjörk D, Ihalainen P, Kaihovirta N, Österbacka R, Peltonen J and Toivakka M 2009 A multilayer coated fiber-based substrate suitable for printed functionality *Org. Electron.* **10** 1020–3

[12] Härting M, Zhang J, Gamota D R and Britton D T 2009 Fully printed silicon field effect transistors *Appl. Phys. Lett.* **94** 193509

[13] Yang L, Zhang R, Staiculescu D, Wong C P and Tentzeris M M 2009 A novel 'green' fully-integrated ultrasensitive RFID-enabled gas sensor utilizing inkjet-printed antennas and carbon nanotubes *IEEE Antennas Wirel. Propag. Lett.* **8** 653–6

[14] Mannerbro R, Ranlöf M, Robinson N and Forcheimer R 2008 Ink-jet printed electrochemical organic electronics *Synth. Met.* **158** 556–60

[15] Rebros M, Hrehorova E, Bazuin B J, Joyce M K, Fleming P D and Pekarovicova A 2008 *Rotogravure* printed UHF RFID antennae directly on packaging materials *Proc. Technical Association of the Graphic Arts (TAGA) (San Francisco) (March 16–18)*

[16] Borisov S M and Wolfbeis O S 2008 Optical biosensors *Chem. Rev.* **108** 423–61

[17] Zang D, Ge L, Yan M, Song X and Yu J 2012 Electrochemical immunoassay on a 3D microfluidic paper-based device *Chem. Commun.* **48** 4683–5

[18] Nie Z, Nijhuis C A, Gong J, Chen X, Kumachev A, Martinez A W, Narovlyansky M and Whitesides G M 2010 Electrochemical sensing in paper-based microfluidic devices *Lab Chip* **10** 477–83

[19] Dungchai W, Chailapakul O and Henry C S 2009 Electrochemical detection for paper-based microfluidics *Anal. Chem.* **81** 5821–6

[20] Ihalainen P *et al* 2013 Application of paper-supported printed gold electrodes for impedimetric immunosensor development *Biosensors* **3** 1–17

[21] Määttänen A, Vanamo U, Ihalainen P, Pulkkinen P, Tenhu H, Bobacka J and Peltonen J 2013 Low-cost paper-based inkjet-printed platform for electrochemical analysis *Sensors Actuators* B **177** 153–62

[22] Ihalainen P, Majumdar H, Määttänen A, Wang S, Österbacka R and Peltonen J 2013 Versatile characterization of thiol-functionalized printed metal electrodes on flexible substrates for cheap diagnostic applications *Biochim. Biophys. Acta* **1830** 4391–7

[23] Rusling J F, Hvastkovs E G and Schenkman J B 2007 Toxicity screening using biosensors that measure DNA damage *Curr. Opin. Drug Discov. Devel* **10** 67–73

[24] Takacs K, Nemedi E, Marta D, Gelencder T and Kovacs E T 2007 Use of the enzyme transglutaminase for developing glutenfree noodle products from pea flour *Acta Alimentaria* **36** 195–205

[25] Waggoner P S and Craighead H G 2007 Micro- and nanomechanical sensors for environmental, chemical and biological detection *Lab Chip* **7** 1238–55

[26] Patolsky F, Zheng G and Lieber C M 2006 Nanowire sensors for medicine and the life sciences *Nanomedicine* **1** 51–65

[27] White D C, Gouffon J S, Peacock A D, Geyer R, Biernacki A, Davis G A, Pryor M, Tabacco M B and Sublette K L 2003 Forensic analysis by comprehensive rapid detection of pathogens and contamination concentrated in biofilms in drinking water systems for water resource protection and management *Environ. Forensics* **4** 63–74

[28] Bonanni A and del Valle M 2010 Use of nanomaterials for impedimetric DNA sensors: a review *Anal. Chim. Acta* **678** 7–17

[29] Tosar J P, Branas G and Laiz J 2010 Electrochemical DNA hybridization sensors applied to real and complex biological samples *Biosens. Bioelectron.* **26** 1205–17

[30] Prodromidis M I 2010 Impedimetric immunosensors—a review *Electrochim. Acta* **55** 4227–33

[31] Berggren C, Bjarnason B and Johansson G 2001 Capacitive biosensors *Electroanalysis* **13** 173–80

[32] Janek R P, Fawcett W R and Ulman A J 1997 Impedance spectroscopy of self-assembled monolayers on Au(111): evidence for complex double-layer structure in aqueous $NaClO_4$ at the potential of zero charge *J. Phys. Chem.* B **101** 8550–8

[33] Hubrecht J 1988 Electrochemical impedance spectroscopy as a surface analytical technique for biomaterials *Metals as Biomaterials* ed J A Helsen and J Breme (New York: Wiley) pp 405–66

[34] Berggren C, Stålhandske P, Brundell J and Johansson G 1999 A feasibility study of a capacitive biosensor for direct detection of DNA hybridization *Electroanalysis* **11** 156–60

[35] Wei F, Sun B, Guo Y and Zhao X S 2003 Monitoring DNA hybridization on alkyl modified silicon surface through capacitance measurement *Biosens. Bioelectron.* **18** 1157–63

[36] Berney H, West J, Haefele E, Alderman J, lane W and Collins J K 2000 A DNA diagnostic biosensor: development, characterisation and performance *Sensors Actuators* B **68** 100–8
[37] Cai W, Peck J R, van der Wiede D W and Hamers R J 2004 Direct electrical detection of hybridization at DNA-modified silicon surfaces *Biosens. Bioelectron.* **19** 1013–9
[38] Yang W, Butler J E, Russel J N Jr and Hamers R J 2004 Interfacial electrical properties of DNA-modified diamond thin films: intrinsic response and hybridization-induced field effects *Langmuir* **20** 6778–87
[39] Lee T-Y and Shim Y-B 2001 Direct DNA hybridization detection based on the oligonucleotide-functionalized conductive polymer *Anal. Chem.* **73** 5629–32
[40] Gu H, di Su X and Loh K P 2005 Electrochemical impedance sensing of DNA hybridization on conducting polymer film-modified diamond *J. Phys. Chem.* B **109** 13611–8
[41] Bollström R, Määttänen A, Ihalainen P, Peltonen J and Toivakka M 2010 *Method for Creating a Substrate for Printed or Coated Functionality, Substrate, Functional Device and its Use PCT/FI2010/050056* WO 2010/086511
[42] Määttänen A, Ihalainen P, Bollström R, Toivakka M and Peltonen J 2010 Wetting and print quality study of an inkjet-printed poly(3-hexylthiophene) on pigment coated papers *Colloids Surf.* A **367** 76–84
[43] Hostetler M J *et al* 1998 Alkanethiolate gold cluster molecules with core diameters from 1.5 to 5.2 nm: core and monolayer properties as a function of core size *Langmuir* **14** 17–30
[44] Määttänen A, Fors D, Wang S, Valtakari D, Ihalainen P and Peltonen J 2011 Paper-based planar reaction arrays for printed diagnostics *Sensors Actuators* B **160** 1404–12
[45] Mir M, Alvarez M, Azzaroni O and Knoll W 2008 Comparison of different supramolecular architectures for oligonucleotide biosensing *Langmuir* **24** 13001–6
[46] Su X, Wu Y-J, Robelek R and Knoll W 2005 Surface plasmon resonance spectroscopy and quartz crystal microbalance study of streptavidin film structure effects on biotinylated DNA assembly and target DNA hybridization *Langmuir* **21** 348–53
[47] Su X, Wu Y-J and Knoll W 2005 Comparison of surface plasmon resonance spectroscopy and quartz crystal microbalance techniques for studying DNA assembly and hybridization *Biosens. Bioelectron.* **21** 719–26
[48] Lee C-Y, Gong P, Harbers G M, Grainger D W, Castner D G and Gamble L J 2006 Surface coverage and structure of mixed DNA/alkylthiol monolayers on gold: characterization by XPS, NEXAFS, and fluorescence intensity measurements *Anal. Chem.* **78** 3316–25
[49] Herne T M and Tarlov M J 2005 Characterization of DNA probes immobilized on gold surfaces *J. Am. Chem. Soc.* **119** 8916–20
[50] Barsoukov E and Macdonald J R (ed) 2005 *Impedance Spectroscopy Theory, Experiment, and Applications* 2nd edn (New Jersey: Wiley)
[51] Van Oss C J, Giese R F, Bronson P M, Docoslis A, Edwards P and Ruyechan W T 2003 Macroscopic-scale surface properties of streptavidin and their influence on aspecific interactions between streptavidin and dissolved biopolymers *Colloids Surf.* B **30** 25–36
[52] Myland J C and Oldham K B 2000 Uncompensated resistance. 1. The effect of cell geometry *Anal. Chem.* **72** 3972–80
[53] Xing Y F, Li S F Y, Lau A K H and O'Shea S J 2005 Electrochemical impedance spectroscopy study of mixed thiol monolayers on gold *J. Electroanal. Chem.* **583** 124–32
[54] Boubour E and Lennox R B 2000 Insulating properties of self-assembled monolayers monitored by impedance spectroscopy *Langmuir* **16** 4222–8
[55] Souteyrand E, Martin J R and Martelet C 1994 Direct detection of biomolecules by electrochemical impedance measurements *Sensors Actuators* B **20** 63–9
[56] Kelley S O and Barton J K 1999 Electron transfer between bases in double helical DNA *Science* **283** 375–81
[57] Lin K-C, Kunduru V, Bothara M, Rege K, Prasad S and Ramakrishna B L 2010 Biogenic nanoporous silica-based sensor for enhanced electrochemical detection of cardiovascular biomarkers proteins *Biosens. Bioelectron.* **25** 2336–42
[58] Limbut W, Kanatharana P, Mattiasson B, Asawatreratanakul P and Thavarungkul P A 2006 Comparative study of capacitive immunosensors based on self-assembled monolayers formed from thiourea, thiotic acid, and 3-mercaptopropionic acid *Biosens. Bioelectron.* **22** 233–40
[59] Limbut W, Kanatharana P, Mattiasson B, Asawatreratanakul P and Thavarungkul P A 2006 Reusable capacitive immunosensor for carcinoembryonic antigen (CEA) detection using thiourea modified gold electrode *Anal. Chim. Acta* **561** 55–61
[60] Multon S E, Barisci J N, Bath A, Stella R and Wallace G G 2004 Studies of double layer capacitance and electron transfer at a gold electrode exposed to protein solutions *Electrochim. Acta* **49** 4223–30
[61] Sibai A, Elamri K, Barbier D, Jaffrezic-Renault N and Souteyrand E 1996 Analysis of the polymer–antibody–antigen interaction in a capacitive immunosensor by FTIR difference spectroscopy *Sensors Actuators* B **31** 125–30